



# Experimental mechanistic investigation of the nanostructuring of tungsten with low energy helium plasmas



P. Fiflis\*, N. Connolly, D.N. Ruzic

Center for Plasma Material Interactions, Department of Nuclear, Plasma and Radiological Engineering, University Illinois at Urbana-Champaign, Urbana, IL, 61801, USA

## ARTICLE INFO

### Article history:

Received 24 May 2016

Received in revised form

17 August 2016

Accepted 6 October 2016

Available online 8 October 2016

## ABSTRACT

Helium ion bombardment of tungsten at temperatures between approximately one third and one half of its melting point has shown growth of nanostructures colloquially referred to as “fuzz”. The nanostructures take the form of thin tendrils of diameter about 30 nm and grow out of the bulk material. Tungsten will and does compose one of the key materials for plasma facing components (PFCs) in fusion reactors. The formation of nanostructured fuzz layers on PFCs would be detrimental to the performance of the reactor, and must therefore be avoided. Previous experiments have shown evidence that tungsten fuzz is initially grown by loop punching of helium bubbles created in the bulk. However, once the tendrils grow to sufficient length, the tendrils should intercept the entire helium flux, halting the production of fuzz. Fuzz continues to grow though. To increase the understanding of the mechanisms of tungsten fuzz formation, and thereby aid the avoidance of its production, a series of tests were performed to examine the validity of several theories regarding later stage tungsten fuzz growth. Tests showed that the fuzz formation was dependent solely on the bombardment of helium ions, and not on electric fields, or adatom diffusion. Experiments employing a tungsten coated molybdenum sample indicate the presence of a strong mixing layer and strongly suggest that tungsten fuzz growth continues to occur from the bottom up even as the tendrils grow in size. Tests also show a similarity between different metals exposed to helium ion fluxes where the ratio of bubble diameter to tendril diameter is constant.

© 2016 Elsevier B.V. All rights reserved.

## 1. Introduction

Tungsten under exposure to a sufficiently energetic (greater than 20 eV) flux of helium ions between the temperatures of 1000K and 2000K will undergo a surface modification which results in growth of nanotendrils out of the bulk of the material, eventually culminating in a layer of nanostructured tungsten with a volume averaged density much less than that of the bulk tungsten [1–3]. Nanostructuring of tungsten has been studied extensively due to its importance to the plasma-material interface in fusion reactors [4]. This nanostructured tungsten is a porous structure with greatly enhanced surface area, increased emissivity, greater light absorption, and reduced sputtering yields [2,5,6]. Many experiments have been performed showing the envelope of conditions under which tungsten fuzz is created, and still more have been performed to

elucidate the mechanisms behind its formation. It has been the conclusion of several studies that the initial formation of the fuzz is driven by the formation of bubbles in the bulk from helium implantation, whether by self-nucleation [7] or clustering at defects [8]. These bubbles then loop-punch to the surface of the tungsten, forming craters or pits in the surface [9–13]. Buildup of pits on the surface eventually reaches a critical level, beyond which hillocks and valleys begin to form [14]. The time required to reach this critical level may explain the observation of an “incubation time” or “incubation fluence” which refers to the non-zero fluence intercept proposed by studies concerning the growth rate of tungsten fuzz [3]. Subsequently, the hillocks then sharpen into tendrils which continue to grow from the surface [14]. One outstanding question, however, remains. As these tendrils continue to grow from the surface, the incoming helium flux will begin to be intercepted by the protruding tendrils rather than the bulk. Without a source of helium ions, bubble formation in the bulk will be suppressed. The question therefore remains, what continues to drive the formation of tungsten fuzz at thicknesses greater than that whereby all of the

\* Corresponding author.

E-mail address: [fiflis1@illinois.edu](mailto:fiflis1@illinois.edu) (P. Fiflis).

helium ions are intercepted by protruding tendrils?

## 2. Potential mechanisms

Several theories have been proposed to explain the continuation of tungsten fuzz formation. The first of these is that the originally implanted bubble layer is sufficient for nanotendrils formation. According to this theory, an initial layer of tungsten is impregnated with helium. This layer then “froths” up via the loop punching mechanism to form the tendrils. One of the key implications of this theory is that the mass of the tungsten fuzz layer would remain constant. This implication is experimentally supported by measurements of the average porosity of the fuzz layer as a function of the thickness of the layer which seem to indicate that the mass of the fuzz remains constant [3].

Many of the remaining theories make use of a two mechanism system. For these, loop punching of bubbles is responsible for the first stages of formation and is then eclipsed by a second mechanism as helium becomes intercepted by tungsten fuzz tendrils rather than the bulk metal. Experimental evidence supports this assumption insofar as that fuzz formation occurs with a growth rate of time to the  $\frac{1}{2}$  power after some initial incubation time. Nucleation of some structure on the surface is a critical precursor to all of the following proposed theories.

Another is that the growth of the nanostructured layer is driven by the migration of adatoms on the surface of the tungsten [15]. Adatoms are generated by the bombardment of helium ions, and it is more energetically favorable for the adatoms to come to rest on the top of a tendril rather than at the base or on the bulk surface. Nucleation of the tendrils in this case may still be driven by the loop punching mechanism discussed earlier, however, continued growth is driven by the movement of generated adatoms on the surface.

The third theory is electrostatic growth of the tungsten tendrils. Interplay between a generated dipole moment in the fuzz tendril and the strong sheath electric field may exert sufficient force on the tendril to draw it from the bulk, similar to metal whisker formation in RF devices [16]. This would also rely on nucleation of tendrils via loop punching.

Next, it has been proposed that growth of the tungsten tendrils is driven by viscoelastic flow of tungsten up the tendril from the bulk [17]. According to this theory, large stresses induced by the presence of bubbles in the tendrils cause enhanced plastic flow of tungsten such that tungsten flows around the bubbles to grow the tendril. Furthermore, this process is rate limited by the flow of tungsten from the bulk such that the growth rate of the tendrils becomes proportional to  $t^{1/2}$ .

A final theory, clearly elucidated here for the first time, suggests that continuation of the growth of nanostructured tungsten tendrils continues to be driven by the same mechanism that initiated the growth: loop punching of helium bubbles in the bulk to the surface. The source of the helium to continue generating the bubbles, however, is a matter of some question as direct impingement of helium on the bulk tungsten is decreased as the tendrils begin to shadow the surface. The source of helium may derive from helium diffusion down the tendril after impingement higher up on the tendril. The compressive stress fields around helium bubbles in the tendrils may serve to channel helium down the channel and into the bulk [18]. It may also be that simple diffusion of helium down the tendrils, while very small, is still sufficient to drive growth.

This study was performed to investigate the validity of the above outlined theories and to help elucidate other potential mechanisms. Tungsten wires were exposed to multiple different experimental conditions to differentiate between sheath electric field, temperature, and ion bombardment effects. Next, tungsten coated

molybdenum wires and strips were exposed to the helium helicon plasma to investigate the transport of the tungsten relative to the molybdenum. By investigating the atomic composition of the nanostructured tendrils and the spatial dependence of the tungsten/molybdenum ratio, information was gleaned on the source of material fueling nanotendrils growth. Molybdenum was chosen as the substrate for the deposited tungsten layer because of the similar lattice constant (for adhesion of the deposited layer) and because of the similar conditions and morphologies observed in the nanostructuring of molybdenum and tungsten. Finally, several other materials, namely, copper, tantalum, molybdenum, and titanium were also exposed to helium ion fluences to investigate the similarity or difference of the formation of nanostructures on these materials to tungsten. Previous studies have suggested a dependence of nanostructuring on crystal structure [19,20].

## 3. Experimental setup

Wires of tungsten, copper, tantalum, molybdenum, and titanium (Alfa Aesar 99.9%) were exposed in a helium helicon source (MORI 200 [21]). Plasma conditions for the exposures are identical to past studies performed at the University of Illinois on the growth of tungsten nanostructures and palladium nanostructures [14,22]: An RF power of 700W, a magnetic field of 120G, and a background helium pressure of 100 mTorr as read by a convectron gauge (Granville Phillips 375), a plasma density of  $1e18 \text{ m}^{-3}$  and an electron temperature of 4 eV as diagnosed by an RF-compensated Langmuir probe [23] in the region where the sample was placed. Samples were biased to negative 20V relative to ground. Plasma potential was found to be positive 20V relative to ground via Langmuir probe measurements. Consequently, the incoming helium ion flux had an energy of 40 eV. The flux helium ions was  $2.5e21 \text{ m}^{-2}\text{s}^{-1}$ . Sample temperatures were achieved by a combination of heating by the incoming flux of helium ions as well as resistive heating by passing a current through the wire. Temperatures were not directly measured, but rather computed via a calibrated finite difference model which balances input energy from helium ion irradiation and losses via conduction and radiation [14,22]. The exposure temperature of the samples exposed here computed from this model was 1100 K. Scanning electron microscopy (Hitachi S4700) was performed on the exposed samples. Energy dispersive x-ray spectroscopy (EDX) was also performed to confirm that the tendrils observed on the surface of the various materials did indeed match the bulk material.

Several tests were performed on a set of tungsten wires to investigate the proposed two mechanism growth of tungsten fuzz discussed previously. Nucleation of tungsten fuzz tendrils was driven conventionally in the method described above to the hills and valleys stage of nanostructure formation [14]. SEM micrographs of samples at this stage of formation are shown in Fig. 1. Following this, the tungsten wires were immediately subjected to an additional process to see if nanostructure growth would continue.

The first of these two processes was to investigate if only the initial stages were driven by helium bubbles, and to see if an identical plasma, only with a different gas would have an effect, the sample was driven after the hills and valleys stage with both hydrogen and neon as process gases. In each case, the current in the wire was reduced to zero, and the plasma extinguished. The process gas was then switched immediately without breaking vacuum, the plasma was reignited and the current restored. In each case, the electron density and temperature were matched to that of the helium case such that the ion flux to the wire would be identical to the ion flux of helium previously. The samples were then exposed for 25 h.

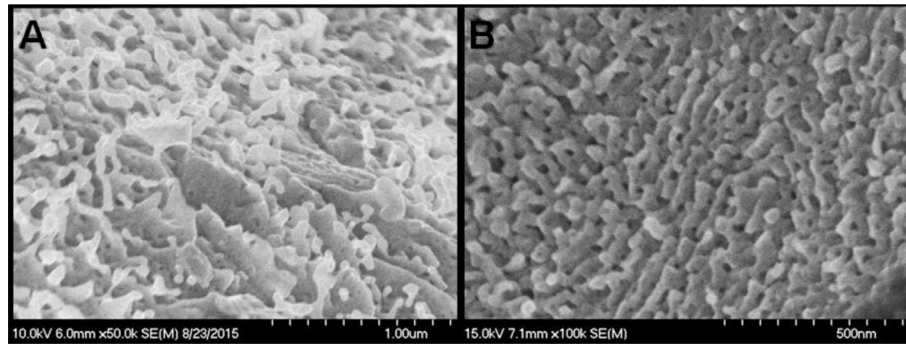


**Fig. 1.** SEM micrographs of two tungsten wires exposed just beyond the hills and valleys stage of tungsten fuzz formation. 1-A is inclined, the view of 1-B is normal to the surface. It can be seen that the hills are just starting to narrow into tendrils, and the tendrils have yet to grow to sufficient length and convolution to obscure the bulk from helium ion bombardment.

The second of these processes simulated the effect of the strong electric field present in the plasma sheath with a DC bias. The wire was first prepared to the hills and valleys stage. After allowing the wire to cool, the sample was removed from vacuum and placed in a sample holder consisting of an aluminum tube (2 cm ID, Alloy 6061, McMaster Carr) and two ceramic (Macor, McMaster Carr) endcaps. The wire was suspended by the ceramic endcaps on the axis of the aluminum tube. A schematic and photo of the experimental setup can be seen in Fig. 2. The setup was placed in the body of the helicon chamber described herein, and the chamber evacuated and backfilled to 100 mTorr of helium. A 2.5 kV bias was applied between the cylinder and the wire. The field was chosen to match the applied electric field to the average sheath electric field in the plasma. Due to the short distance between the wire and the cylinder, no breakdown occurred. The wire was heated via passing a current through it to 1100 K. The wire was subsequently exposed for 25 h.

Finally, molybdenum wires (99.9% Alfa Aesar) were coated with tungsten by sputter magnetron (2" gun, Kurt J Lesker, 3 mTorr Argon) to thicknesses of  $105 \pm 5$ ,  $320 \pm 15$ , and  $1060 \pm 50$  nm at temperature of 625 K and subsequently were exposed to plasmas of identical conditions as described above. Molybdenum strips (0.1 mm thick, 2 mm wide, 99.9% Alfa Aesar) were also similarly coated with tungsten by sputter magnetron to thicknesses of  $100 \pm 5$ ,  $200 \pm 10$ ,  $500 \pm 25$ , and  $1000 \pm 50$  nm and identically exposed. Molybdenum was chosen as the substrate to investigate material transport for the similarity of its nanostructure morphology to tungsten as well as its similar temperature window for creation, and similar lattice constant. The deposition rate was

measured by profilometry (DEKTAK 3030) on a masked silicon wafer exposed to identical sputter conditions. Deposition rate was found to be  $800 \pm 40$  nm over 15 min. After plasma exposure, the wires and strips were similarly examined with SEM, Auger electron spectroscopy (AES) to investigate the relative transport of the different materials.

## 4. Results and discussion

### 4.1. Gas replacement and electric field tests

SEM micrographs of the tungsten wire exposed to the hills and valleys stage can be seen in Fig. 1. SEM micrographs of the tungsten after exposure to the hills and valleys stage with helium as the plasma process gas and subsequent exposure with hydrogen and neon as the process gases are shown in Fig. 3A and B respectively. For comparison, a tungsten wire exposed continuously with helium as the process gas is shown in Fig. 3C. It can be seen that tungsten nanostructures readily grow in the case of helium plasma exposure, however, neither the exposure to hydrogen nor to neon caused significant growth of nanostructures. The hydrogen exposure looks little different than the tungsten only exposed to the hills and valleys stage. In the neon structure the hills and valleys look to have partially subsided. The sputtering threshold of neon on tungsten is approximately 45 eV [24], and since the energy of the ion flux was 40 eV, the smoothing of the initially roughened surface is attributed to beam enhanced surface diffusion similar to the annealing of tungsten nanostructures observed on NAGDIS [5]. Even with the same sheath geometry, magnitude of ion flux, and material

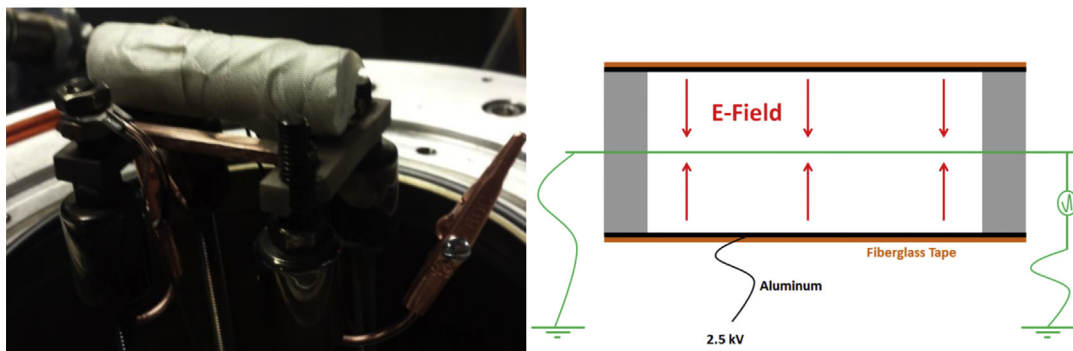


**Fig. 2.** Experimental setup for electric field tests (photo left, schematic right). Structure consisting of four threaded rods attached to a plate at the bottom of the chamber suspend the sample holder in the bell jar that sits within the MORI source. Aluminum tube shown here coated in fiberglass tape to prevent discharge to other surfaces within the vacuum chamber. Ceramic endcaps on both ends suspend tungsten wire within tube. Copper alligator clips used to ground tungsten wire while aluminum tube biased to positive potential.

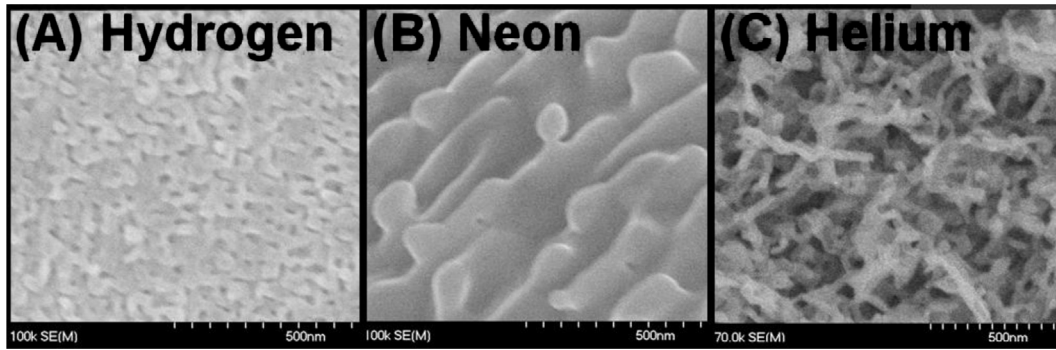


**Fig. 3.** Comparison of tungsten wires exposed in gas replacement tests. No evidence of further nanostructuring can be seen in either the hydrogen or neon cases. The reference helium case however, shows continued nanostructuring well beyond the hills and valleys stage.

temperature, nanostructure growth is not promoted by either hydrogen or neon, showing that helium is important to the process throughout.

Wires of tungsten before and after exposure to a DC electric field test to simulate a sheath electric field without a plasma as described above yet after exposure just past the hills and valleys stage can be seen in the SEM micrographs in Fig. 4A and B respectively. In these tests, the tungsten wire was at the same temperature as the plasma exposures, in an environment of hot helium gas and similar electric field, but without ion bombardment as there was no plasma breakdown. From these micrographs, another null result can be seen. No further nanostructuring was observed on these wires beyond the hills and valleys stage of tungsten fuzz formation. The combination of these electric field tests and the gas replacement tests above give strong evidence against two of the theories discussed previously, namely, the theory that further growth of tungsten fuzz is driven by adatom migration on the surface of the tungsten, and the theory that the growth is due to an electrostatic interaction between the tendrils and the sheath electric field. If either of these were the case, they would have showed a positive result in the gas replacement tests. Bombardment by either 40 eV hydrogen or neon would generate adatoms on the surface due to knockout from the surface layer similar to helium bombardment, and if this were the process, the growth of the nanostructures would be insensitive to the process gas at this stage. Similarly, in plasmas of both hydrogen and neon of similar density and temperature to the helium plasmas used in previous experiments, the sheath electric field structure would be very similar, and therefore, if the mechanism were electrostatic growth of the tendrils, both the gas replacement and electric field tests would show a positive result. These tests however do

conclusively prove that the growth of tungsten nanotendrils is solely driven when the wire is at an elevated temperature by the bombardment of an energetic helium ion flux.

#### 4.2. Tungsten coated molybdenum tests

An SEM micrograph of the formed fuzz layer on the 320 nm sample can be seen in Fig. 5. The fuzz layers on each wire looked identical to those produced on bulk tungsten wires. The AES spectra of the 3 samples exposed as well as a molybdenum wire sputter-

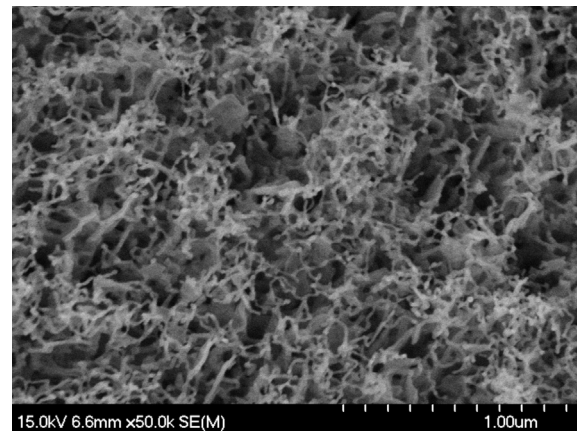


**Fig. 5.** SEM image of tungsten fuzz from tungsten layer deposited on molybdenum wire. Sample shown is from 320 nm tungsten layer. Morphology is identical to tungsten grown from pure tungsten wires as well as the morphology observed on the 105 and 1060 nm deposition samples.

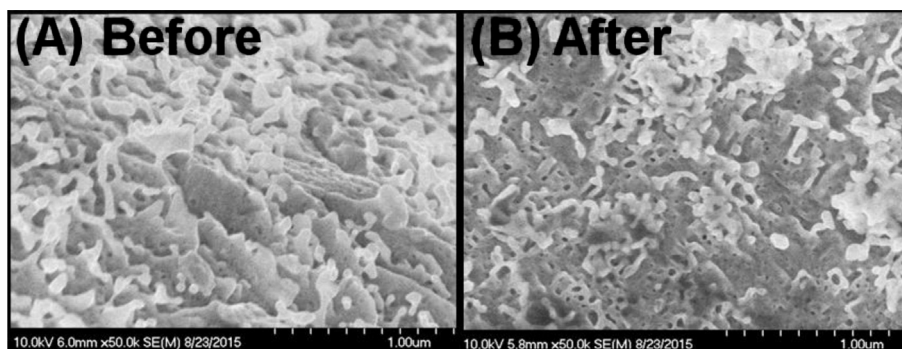


**Fig. 4.** Comparison of tungsten wires exposed in electric field tests. No evidence of further nanostructuring can be seen in this case. A comparison between the two micrographs shows that they are at the same phase of tungsten fuzz growth where hills are narrowing into tendrils.

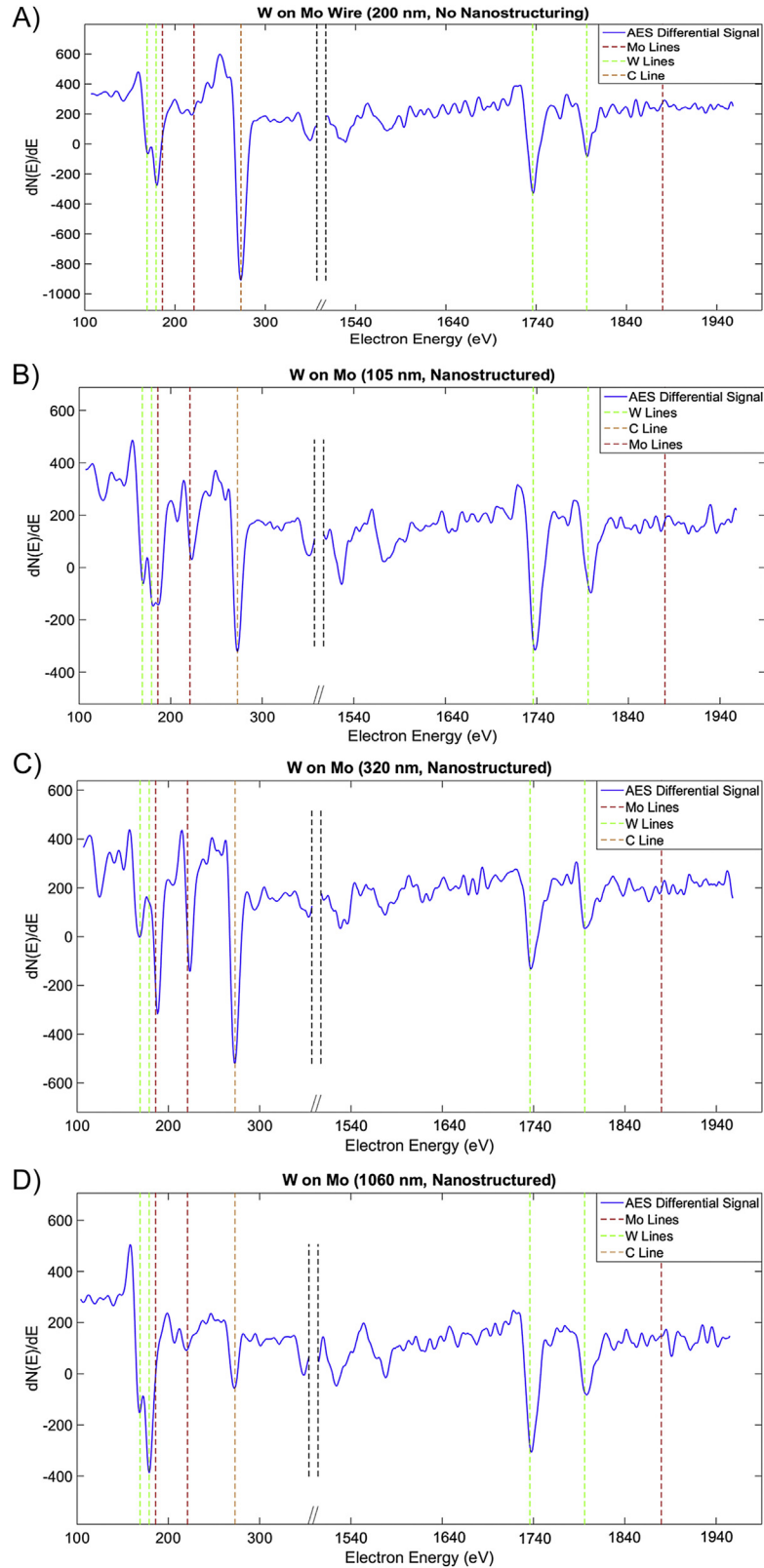


**Fig. 6.** A: AES spectrum of W coated Mo wire without nanostructuring. Provided for reference. Strong tungsten peaks can be observed (as well as a carbon peak, but no molybdenum is observed). Axis broken for clarity. B: Tungsten coated molybdenum wire (105 nm thickness), nanostructured. AES spectrum shows both tungsten and molybdenum lines (weak Mo peak at 1880 eV not observed). C: Tungsten coated molybdenum wire (320 nm thickness), nanostructured. AES spectrum still shows both tungsten and molybdenum lines (weak Mo peak at 1880 eV not observed). D: Tungsten coated molybdenum wire (1060 nm thickness), nanostructured. AES spectrum shows disappearance of molybdenum lines. Only tungsten lines are observed.

coated with tungsten, but not nanostructured, for reference can be seen in Fig. 6. From these AES spectra, it can be seen that molybdenum is being incorporated into the tungsten tendrils when it is available as a source from the bulk. AES is a very surface sensitive technique, as a result of the limited penetration of the incident electron beam as well as the limited range of the Auger electrons in solids. The range of Auger electrons in metals is of order of 10's of Angstroms. So, AES only is able to look at the top few atomic layers. Strong molybdenum signals can be seen from the wires with depositions of 105 and 320 nm. The molybdenum signals are absent however, from both the wire with no nanostructuring (indicating that the tungsten coating is good) as well as the 1060 nm deposition with nanostructuring (indicating that there is a maximum interaction depth between the nanostructuring process and the wire). The inclusion of molybdenum into the tungsten nanostructures at tungsten thicknesses in excess of 50 nm shows that material is being sourced to the tendrils from the bulk even beyond the initial interaction layer of approximately 100 nm [25]. Furthermore, the tungsten coated molybdenum strips were investigated with AES as well. The strips were depth profiled in the AES by sputtering with a 3 keV argon ion gun. The tungsten concentration as a function of depth for the 100, 200 and 500 nm

samples is shown in Fig. 7. Multiple observations can be drawn from this figure. First among these is that the helicon plasma erodes some of the tungsten from the surface by sputtering. The eroded thickness can be estimated from the fluence-thickness relationship provided in T.J. Petty et al. [3] as approximately  $75 \pm 20$  nm. This can be seen in the greatly reduced tungsten counts in the 100 nm sample as compared to the 200 and 500 nm samples. The next of these observations is that growth of fuzz appears to be continued by molybdenum from the bulk further pushing the tendrils outward, rather than molybdenum being drawn up the sides of the tendril to the top to continue to grow the fuzz layer. This is evidenced by the transition from tungsten rich to molybdenum rich seen in the 200 nm sample within the fuzz layer as the fuzz layer is traversed from top to bottom. If material were being drawn up the sides of the tendril to grow the fuzz, tungsten would be present throughout the fuzz, rather than only at the top. The final observation is that a series of sigmoid fits to each of the W/Mo data sets each display the same e-folding length of approximately 250 nm. This indicates the presence of a strong mixing layer between the molybdenum and the tungsten. Taking the thickness of this mixing layer as an e-folding length on either side of the inflection point of the sigmoid, this mixing layer between tungsten and molybdenum

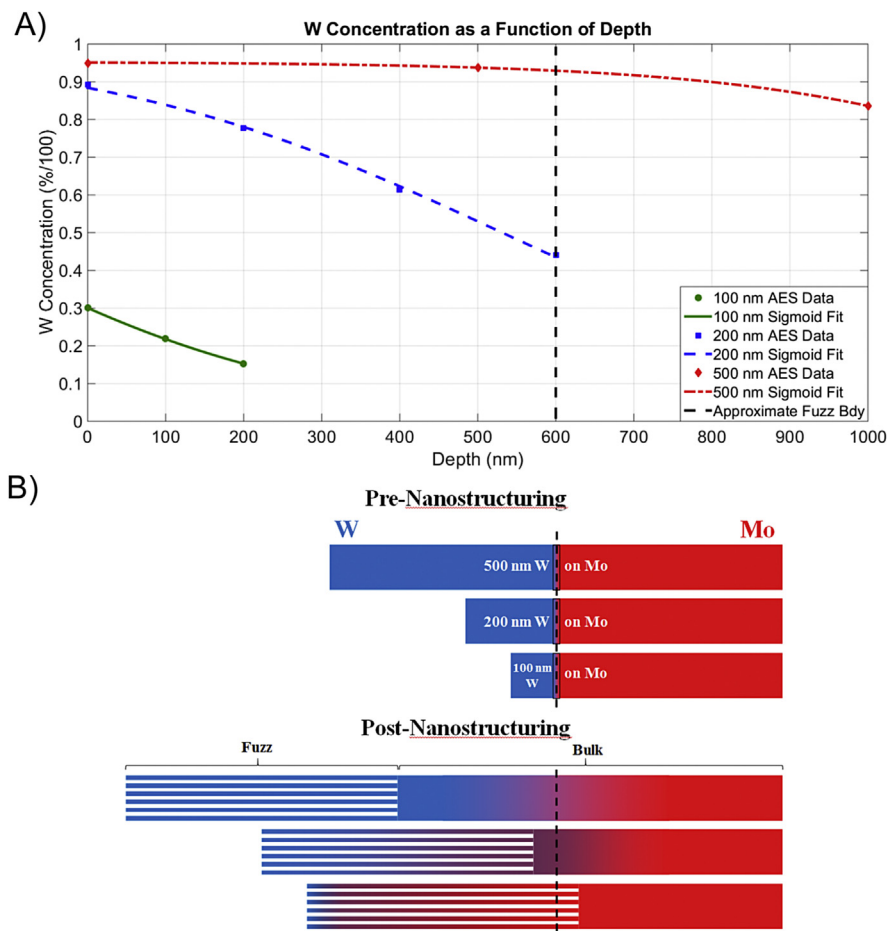


**Fig. 7.** A: Ratio of tungsten to molybdenum counts for AES spectra on 100, 200 and 500 nm tungsten coated molybdenum samples. Decreasing ratio with increasing depth indicates more molybdenum as the sputtered depth increases. Depth as used here refers to the distance below the top of the fuzzed surface at which the AES measurement was taken. For samples on which 600 nm of fuzz was grown, 0 nm lays at the top of the fuzz layer and 600 nm lays at the fuzz-bulk interface. Sigmoid fit shown as well. E-folding length of sigmoid fit is approximately 250 nm. Transition observed from tungsten rich region to molybdenum rich region indicative of strong layer mixing. B: Visualization of AES data presented in Fig. 7A. Initial state of molybdenum strips coated with tungsten are seen in the top of the figure for the 100, 200 and 500 nm depositions. Tungsten layers are colored blue, molybdenum layers are colored red. The nanostructured samples are visualized in the bottom half of the figure. Mixed layers are depicted by a gradient fill, the bulk layers are depicted as a single solid rectangle, and the fuzz layer is marked by bars with a transparent box behind. (For interpretation of the references to colour in this figure legend, the reader is referred to the web version of this article.)

is approximately 500 nm in thickness, providing evidence that the interaction layer between the nanostructuring process is thicker than originally thought [25]. An AES depth profile of a molybdenum strip coated with 250 nm of tungsten, but not nanostructured shows a transition region less than 16 nm in thickness.

These AES results show strong evidence that material is sourced from the bulk through the tungsten fuzz formation process, and that the interaction layer between the bulk and fuzz tendrils is much deeper than originally thought. They also show that tendrils are continually pushed upward by continued growth at the base. The experimental evidence presented here points to continued loop punching by helium reaching the bulk. Growth of tungsten fuzz tendrils by continued loop punching requires a continued source of helium to the bulk. Per the theory presented earlier, this may be due to diffusion of implanted helium down the tendrils, which may be further enhanced by compressive stress fields around helium bubbles.

#### 4.3. Tantalum, molybdenum, copper and titanium nanostructuring

SEM micrographs of nanostructures formed by helium plasma exposure on tantalum, molybdenum, copper, and titanium can be seen in Figs. 8–11 respectively.

Tantalum and molybdenum wires exposed to the helium plasma generated nanostructures very similar to those observed on tungsten. Tendrils of diameter approximately 20–40 nm were observed. The morphology as seen under an SEM is also indistinguishable from tungsten. Similarly to tungsten, a lower temperature limit for the formation of nanostructures on tantalum and molybdenum was observed at approximately 1000 K. Also, similarly to tungsten, pits of diameter approximately 10 nm were observed as a precursor to the hills and valleys stage.

Exposure of copper to helium plasma produced cones on the surface of the copper of approximately 0.3–0.7  $\mu\text{m}$  in diameter at the base and approximately 1  $\mu\text{m}$  tall at temperatures between  $0.3T_m$  and  $0.5T_m$ . Similar cones have been produced on copper under helium ion bombardment at Pilot PSI [19]. A cross section of the copper exposed at Pilot revealed the presence of voids, presumably due to bubbles, of approximately 70 nm in diameter. Also observed were cones of approximately 240 nm in diameter with an average separation of about 475 nm. Strong similarities can be seen in the ratio of both feature diameter and average feature separation to the observed bubble diameter in the case of helium driven nanostructuring of tungsten, molybdenum, tantalum, copper, and, as noted in a previous study [22], palladium. A table of the various exposed metals, the helium bubble diameter, tendril diameter, and

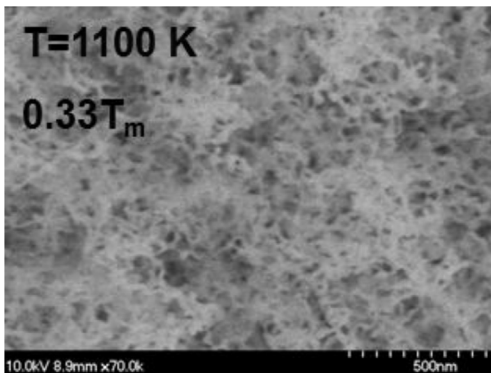


**Fig. 8.** Tantalum surface exposed to helium helicon plasma. The morphology of the tendrils is very similar to that of tungsten. The diameter of the tendrils is approximately 25 nm.

intertendrils separation, as well as crystal type and melting point is shown in Table 1. From this table, it can be seen that while nanostructuring can be driven on both BCC and FCC metals, the helium bubble size is larger in the FCC metals. The difference in size between the FCC and BCC metals is attributed to a difference in the

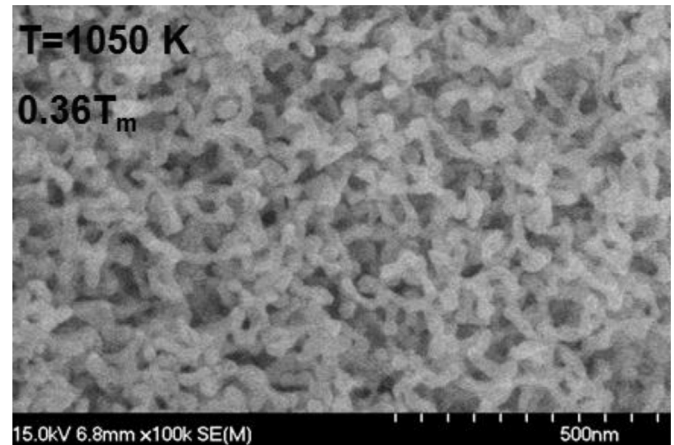


**Fig. 9.** Molybdenum surface exposed to helium helicon plasma. Morphology of the tendrils is very similar to that of tungsten. The diameter of the tendrils is approximately 30 nm, and a similar complex branching morphology is observed.

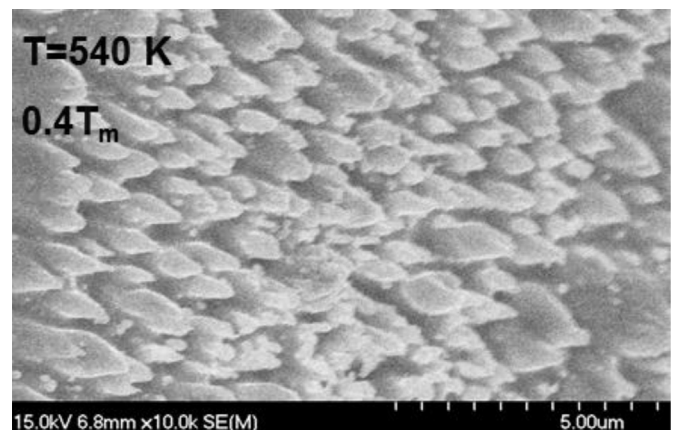


**Fig. 10.** Copper surface exposed to helium helicon plasma. The morphology of the features is cone-like as opposed to tendril-like. The lower temperature limit for copper was not observed, however, the upper temperature limit was, as beyond approximately  $0.67T_m$ , nanostructures appeared to recede back into the surface.

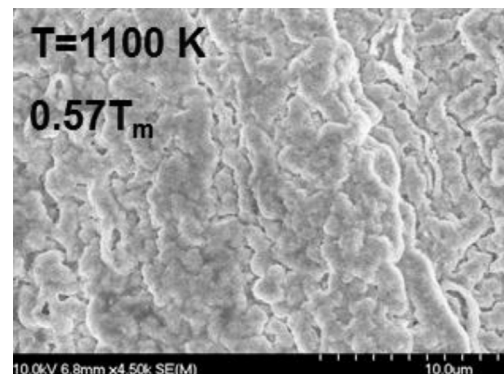


**Fig. 11.** Structuring of titanium by incident helium ions at elevated temperature. Structure is grooved and roughened.

**Table 1**  
Comparison of the pit diameter, tendril diameter, and inter-tendril separation for a variety of metals exposed to helium helicon plasma. Similar ratios are indicative of a common nucleating mechanism.

	Tungsten	Tantalum	Molybdenum	Palladium	Copper
Lattice	BCC	BCC	BCC	FCC	FCC
Melting point	3965 K	3293 K	2896 K	1828 K	1358 K
Shear Modulus	161 GPa	69 GPa	20 GPa	44 GPa	48 GPa
Surface Energy (min)	1.806 eV/atom	1.531 eV/atom	1.534 eV/atom	0.824 eV/atom	0.707 eV/atom
Pit (Bubble) Size	10 nm	10 nm	10 nm	100 nm	70 nm
	1×	1×	1×	1×	1×
Tendril Size	20–40 nm	20–40 nm	20–40 nm	300 nm	240 nm
	2×–4×	2×–4×	2×–4×	3×	~3.5×
Intertendril Separation	60–90 nm	60–90 nm	60–90 nm	800 nm	475 nm
	6×–9×	6×–9×	6×–9×	8×	~6.95×

number of helium traps created with each incident helium ion. Due to the increased plasticity of fcc metals, this parameter is larger in these metals, and as a result, the number of helium traps created per incident helium is larger, and therefore the bubble diameter is larger [7]. However, the ratios of the tendril diameter and inter-tendril separation to the bubble diameter in each is in agreement implying that a similar mechanism drives the formation in each case.

## 5. Summary

From the experimental evidence shown here, formation of tungsten nanostructures relies on a two-mechanism model, one mechanism for the initial nucleation and a second for the continued growth of the fuzz. Furthermore, the existing theories for the continued growth of the fuzz were presented and discussed one by one. The results show strong evidence against theories involving adatom diffusion [15], electrostatically enhanced growth [16], and growth from bubbling of an initial fuzz layer. The two theories remaining are the viscoelastic growth of tendrils by formation of bubbles [17] within the tendril inducing stress on the tungsten to plastically deform it and pull tungsten from the bulk, and the theory presented here that helium bubbles within the tendril may help channel helium down the tendril to the base and into the bulk, continuing the growth of tungsten fuzz from its base by bubble growth and loop punching. Experiments with deposition of a tungsten layer on a molybdenum wire with subsequent nanostructuring favor the latter of these, as it appears from AES analysis of the wires and strips post-exposure that material is sourced from the bulk for a large portion of the nanostructure formation process and that the interaction depth is much deeper than previously thought. However, further experimentation is needed to verify that this is the correct formation mechanism. In addition, a variety of samples of different materials were also exposed to the helium helicon plasma showing strong similarities in initial nucleation mechanism of nanostructures between the various metals. Molybdenum and tantalum were shown to have almost identical morphologies to that of tungsten, with similar temperature thresholds to fuzz formation as well. Samples of bulk palladium (i.e. wire and plate) showed evidence of bubbles of approximate diameter 100 nm and tendrils of approximate diameter 350 nm. The nanostructuring growth mechanism for palladium also appears to be similar to that of tungsten, molybdenum and tantalum, with an active temperature range similar to that of tungsten after normalization to the melting point. However, the diameter of the bubbles is much larger than that of those observed in tungsten. Previous studies of exposure of different metals to energetic helium fluxes at elevated temperatures have suggested that the nanostructuring process is heavily dependent on crystal structure [19]. This is further reinforced by the studies performed herein, as well

as by the copper results, which shown much larger nanostructures, similar to palladium. Body centered cubic (bcc) crystals such as tungsten, molybdenum, and tantalum show very similar nanostructures in both size and morphology. Palladium and copper are face centered cubic (fcc) materials, and therefore, will nanostructure differently than the bcc tungsten. However, since the ratio of tendril diameter to pit diameter as well as the ratio of inter-tendril separation to pit diameter is the same for both tungsten and palladium, it is highly probable that the mechanism for the formation of the nanostructures is the same. The difference in bubble size then is the biggest driver in the difference in observed morphology. This difference being attributed to the difference in clustering dynamics of helium bubbles in the two different crystal structures. Titanium (hcp) further reinforces this theory, as it did not nanostructure like the others, but rather showed signs of grooving and roughening.

## Acknowledgements

The authors would like to thank Dr. Richard Haasch of the Fredrick-Seitz Material Research Lab at the University of Illinois for operating the Auger Electron Spectroscopy facility for the AES experiments presented here. The authors would also like to acknowledge the US Dept. of Energy which funded this research under the project DE-SC0008658.

## References

- [1] M.J. Baldwin, R.P. Doerner, Formation of helium induced nanostructure “fuzz” on various tungsten grains, *J. Nucl. Mater.* 404 (2010) 165–173.
- [2] S. Takamura, N. Ohno, D. Nishijima, S. Kajita, Formation of nanostructured tungsten with arborescent shape due to helium plasma irradiation, *Plasma Fusion Res.* 1 (2006) 051, <http://dx.doi.org/10.1585/pfr.1.051>.
- [3] T.J. Petty, M.J. Baldwin, M.I. Hasan, R.P. Doerner, J.W. Bradley, Tungsten “fuzz” growth reexamined: the dependence of ion fluence in non-erosive and erosive helium plasma, *Nucl. Fusion* 55 (2015).
- [4] G.M. Wright, D. Brunner, M.J. Baldwin, K. Bystrov, R.P. Doerner, B. Labombard, et al., Comparison of tungsten nano-tendrils grown in Alcator C-Mod and linear plasma devices, *J. Nucl. Mater.* 438 (2013) S84–S89.
- [5] S. Kajita, N. Ohno, M. Yajima, J. Kato, Growth annealing equilibrium of tungsten nanostructures by helium plasma in non-eroding regimes, *J. Nucl. Mater.* 440 (2013).
- [6] D. Nishijima, M.J. Baldwin, R.P. Doerner, J.H. Yu, Sputtering properties of “fuzzy” tungsten surfaces, *J. Nucl. Mater.* 415 (2015).
- [7] S.I. Krashennnikov, T. Faney, B.D. Wirth, On helium cluster dynamics in tungsten plasma facing components of fusion devices, *Nucl. Fusion* 54 (2014).
- [8] F.W. Meyer, H. Hijazi, M.E. Bannister, K.A. Unocic, L.M. Garrison, C.M. Parish, Flux threshold measurements of He-ion beam induced nanofuzz formation on hot tungsten surfaces, *Phys. Scr.* T167 (2016).
- [9] A. Lasa, S.K. Tahtinen, K. Nordlund, Loop punching and bubble rupture causing surface roughening: a model for W fuzz growth, *EPL* 105 (2014) 25002.
- [10] A. Lasa, K.O.E. Henriksson, K. Nordlund, MD simulations of onset of tungsten fuzz formation under helium irradiation, *Nucl. Instrum. Methods* 303 (2013) 156–161.
- [11] F. Sefta, K.D. Hammond, N. Juslin, B.D. Wirth, Tungsten surface evolution by helium bubble nucleation growth and rupture, *Nucl. Fusion* 53 (2013).
- [12] F. Sefta, N. Juslin, B.D. Wirth, Helium bubble bursting in tungsten, *J. Appl. Phys.*

- 114 (2013).
- [13] A. Ito, Y. Yoshimoto, S. Saito, A. Takayama, H. Nakamura, Molecular dynamics simulations of a helium bubble bursting on tungsten surfaces, *Phys. Scr.* T159 (2014).
- [14] P. Fiflis, D. Curreli, D.N. Ruzic, Direct time resolved observation of tungsten nanostructured growth due to helium plasma exposure, *Nucl. Fusion* 55 (2015).
- [15] Y.V. Martynenko, M.Y. Nagel, Model of fuzz formation on a tungsten surface, *Plasma Phys. Rep.* 38 (2012) 996–999.
- [16] V.G. Karpov, Electrostatic theory of metal whiskers, *Phys. Rev. Appl.* 1 (2014).
- [17] S.I. Krashenninikov, Viscoelastic model of tungsten “fuzz” growth, *Phys. Scr.* T145 (2011).
- [18] B.D. Wirth, Personal Communication, 2016.
- [19] I. Tanyeli, L. Marot, D. Mathys, M.C.M. van de Sanden, G. De Temmerman, Surface modifications induced by high fluxes of low energy helium ions, *Sci. Rep.* 5 (2015), <http://dx.doi.org/10.1038/srep09779>.
- [20] I. Tanyeli, L. Marot, M.C.M. van de Sanden, G. de Temmerman, Nanostructuring of iron surfaces by low-energy helium ions, *ACS Appl. Mater. Int.* 6 (2014).
- [21] R. Tobe, A. Sekiguchi, M. Sasaki, O. Okada, N. Hosokawa, *Thin Solid Films* vols. 281–282, 1996, pp. 155–158.
- [22] P. Fiflis, M.P. Christenson, N. Connolly, D.N. Ruzic, Nanostructuring of palladium with low temperature helium plasma, *Nanomaterials* 5 (2015).
- [23] D.N. Ruzic, *Electric Probes for Low Temperature Plasmas*, American Vacuum Society Education Committee, 1994.
- [24] Y. Yamamura, H. Tarawa, Energy dependence of ion-induced sputtering yields from monoatomic solids at normal incidence, *At. Data Nucl. Data Tables* 62 (1996).
- [25] S. Kajita, N. Yoshida, R. Yoshihara, N. Ohno, M. Yamagiwa, TEM observation of the growth process of helium nanobubbles on tungsten: nanostructure formation mechanism, *J. Nucl. Mater.* 418 (2011).